High Voltage Gain Interleaved Boost Converter with Neural Network Based MPPT Controller for Fuel Cell Based Electric Vehicle Applications

K. Jyotheeswara Reddy[1], N. Sudhakar[2*]
[1,2]School of Electrical Engineering, VIT University, Vellore, India
([1]jyothireddy.kalvakurthi@gmail.com, [2*]nsudhakar@vit.ac.in)

***Abstract*—** Due to the more vigorous regulations on carbon gas emissions and fuel economy, Fuel Cell Electric Vehicles (FCEV) are becoming more popular in the automobile industry. This paper presents a neural network based Maximum Power Point Tracking (MPPT) controller for 1.26 kW Proton Exchange Membrane Fuel Cell (PEMFC), supplying electric vehicle powertrain through a high voltage-gain DC-DC boost converter. The proposed neural network MPPT controller uses Radial Basis Function Network (RBFN) algorithm for tracking the Maximum Power Point (MPP) of the PEMFC. High switching frequency and high voltage gain DC-DC converters are essential for the propulsion of FCEV. In order to attain high voltage gain, a three-phase high voltage gain Interleaved Boost Converter (IBC) is also designed for FCEV system. The interleaving technique reduces the input current ripple and voltage stress on the power semiconductor devices. The performance analysis of the FCEV system with RBFN based MPPT controller is compared with the Fuzzy Logic Controller (FLC) in MATLAB/Simulink platform.

***Index Terms*—** Fuel Cell Electric Vehicle, High Voltage Gain IBC, PEMFC, MPPT, RBFN.

Nomenclature

V_{FC}	PEMFC output voltage
I_{FC}	PEMFC output voltage
P_{max}	PEMFC Maximum power
I_{max}	PEMFC Maximum current
V_{max}	PEMFC Maximum voltage
T	PEMFC Temperature
G	Water content of the membrane
V_{DC}	DC link voltage
V_{act}	Activation voltage
V_{ohm}	Ohmic over voltage
V_{con}	Concentration over voltage
E_{Nernst}	Open circuit thermodynamic voltage
J	Current density
F	Faraday's Constant
ρ_m	Membrane specific resistivity
D	Duty cycle
R	Universal gas constant
R_C	Proton resistance
R_M	Electron flow equivalent resistance
δ_i	Empirical coefficient of each cell
P_{O2}	Oxygen partial pressure
P_{H2}	Hydrogen partial pressure
C_{O2}	Dissolved oxygen concentration

I. INTRODUCTION

Due to the environmental pollution and finite reserves of fossil fuels, automobile industries are showing more interest in Fuel Cell Electric Vehicles (FCEV). The rapid advancements in power electronics and fuel cell technologies have empowered the significant development in FCEVs [1-2]. Fuel cells have the advantages of clean power generation, high reliability, high efficiency and low noise [3]. Depending on the type of electrolyte substance fuel cells are categorized into different types such as Proton Exchange Membrane Fuel Cell (PEMFC), Alkaline Fuel Cell (AFC), Phosphoric Acid Fuel Cell (PAFC), Solid Oxide Fuel Cell (SOFC) and Molten Carbonate Fuel Cell (MCFC). Among all of these, PEMFCs are dominating the automobile industry due to their low operating temperature and the quick startup [4].

The output voltage of fuel cell depends on membrane water content and cell temperature. Notably, fuel cells have non-linear voltage-current characteristics. Hence, there is only a single unique operating point available for fuel cells with the maximum output voltage and power. The maximum power point tracking (MPPT) technique is necessary to extract the maximum power from the fuel cell at different operating conditions. In the literature, various MPPT techniques are available like perturb and observe (P&O), parctical swarm optimization (PSO), incremental conductance (INC), fuzzy logic control (FLC), sliding mode control, neural network (NN) to track maximum power point (MPP) [5-8]. Among all of these available MPPT algorithms, P&O is simple, popular and easy to implement. P&O [9-11] and incremental conductance methods produce oscillations at steady state which will reduce the efficiency of the fuel cell system. To overcome this problem, fuzzy logic controller and neural network [12] algorithms are introduced to track the MPP with increased efficiency and accuracy. In this paper, radial basis function network (RBFN) base MPPT controller is proposed to track the MPP of the PEMFC.

The powertrain architecture of FCEV is shown in Fig. 1. A stack of PEMFC produces an unregulated low DC output voltage. So a boost or step-up DC-DC converter is required to boost and regulate the PEMFC output voltage. Boost converter is extensively used as a front-end power conditioner for the fuel cell. For low power applications, the

This article has been accepted for publication in a future issue of this journal, but has not been fully edited. Content may change prior to final publication. Citation information: DOI 10.1109/ACCESS.2017.2785832, IEEE Access

conventional boost converter is used as a power electronic interface whereas for high power applications boost converter might not be compatible because of its low current handling capability and thermal management issues [13]. To overcome these problems different high voltage gain DC-DC converters are designed in the literature.

In [14-15], a quadratic boost converter composed of two boost converters is proposed to attain high voltage gain. But, using of two boost converters may reduce the overall efficiency of the system. A cascaded 2-phase interleaved DC-DC boost converter is proposed in [16-17]. However, this topology suffers from poor reliability and less efficiency. In [18-19], a boost converter with voltage multiplier cell is proposed to achieve high voltage gain, but the voltage gain of single multiplier cell is not much enough to drive the powertrain of FCEV. Isolated converters with coupled inductors or high frequency transformers are proposed to achieve high voltage gain in [20-21]. The high voltage gain is achieved by adjusting the transformer turns ratio [22]. However, these isolated converters are more expensive compared to non-isolated DC-DC converters. So, this paper proposes a high voltage gain three-phase non-isolated interleaved boost converter (IBC) for fuel cell applications to attain low switching stress and high voltage gain. Interleaving technique increases the reliability of the fuel cell and provides high power capability.

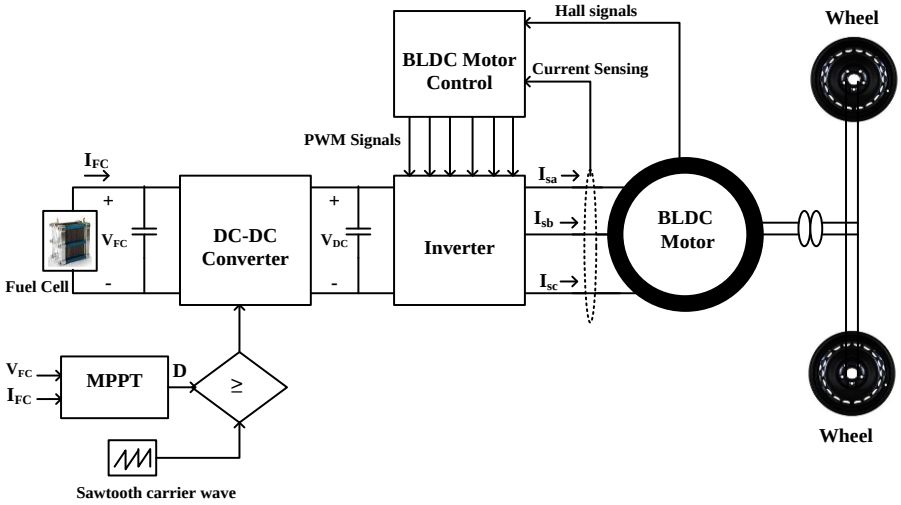

FIGURE 1. Conventional configuration of fuel cell fed BLDC motor driven electric vehicle.

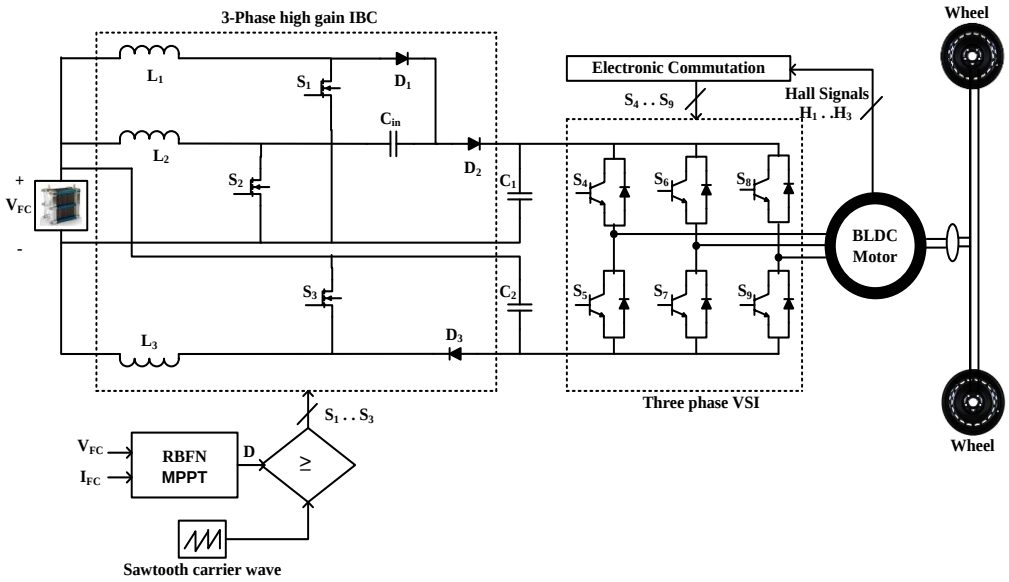

FIGURE 2. Proposed configuration of fuel cell fed BLDC motor driven electric vehicle.

The output voltage of the proposed converter is given to the electric motor through an inverter for propulsion of the vehicle. The electric motor plays an important role in FCEVs. An adequate motor considerably reduces the cost and size of the fuel cell. In past, the majority of automakers are used DC motors for electric vehicle applications. Adversely, DC motors have high maintenance cost and low efficiency due to the brushes and rotating devices [23]. At present, permanent magnet BLDC motor is mostly using in FCEV applications due to simple control, high reliability and high ruggedness [24].

Fig.2 shows the proposed BLDC motor driven FCEV system with three-phase high voltage gain IBC. It consists of a 1.26 kW PEMFC, three-phase high voltage gain IBC, voltage source inverter (VSI) and a BLDC motor. The three-phase IBC operates as an interface between PEMFC and VSI. RBFN based MPPT algorithm is designed to extract the maximum power from the fuel cell. Three-phase IBC supplies power to the BLDC motor through VSI. The switches of the VSI are controlled by using electronic commutation of BLDC motor. The motor shaft is connected to vehicle wheels for the propulsion.

The rest of the paper is organized as follows. PEMFC modeling is discussed in Section II; modeling of the proposed converter is covered in Section III; MPPT and BLDC motor control techniques are described in Section IV; simulations and results are discussed in Section V and the conclusions summarized in Section VI.

II. FUEL CELL MODELING

A fuel cell is an electrochemical device that converts hydrogen fuel into electricity. The inputs to the fuel cell are air and fuel and these are converted into water and electricity through a chemical reaction. A single fuel cell consists of two electrodes (anode and cathode) and an electrolyte. The electrolyte separates the positive and negative charged ions of the hydrogen fuel. When the hydrogen and oxygen are fed into the cell, electricity is generated at the output of the cell in the presence of an electrolyte. Fuel cell produces only heat and water as the wastage of the chemical reaction.

The cell voltage of PEMFC is given as [25-28];

$$V_{FC} = E_{Nernst} - V_{act} - V_{ohm} - V_{con} \quad (1)$$

Where E_{Nernst} is the open-circuit (or reversible) thermodynamic voltage and is given as

$$E_{Nernst} = 1.229 - 8.5\times10^{-4}(T - 298.15) + 4.308\times10^{-5}T\left(ln(P_{H2}) + 0.5ln(P_{O2})\right) \quad (2)$$

Where T is absolute temperature (K), P_{O2} and P_{H2} are oxygen and hydrogen partial pressures (atm) respectively.

Activation voltage V_{act} is the combination of both anode and cathode activation overvoltage and is expressed as

$$V_{act} = -[\delta_1 + \delta_2 T + \delta_3 Tln(C_{O2}) + \delta_4 Tln(I_{FC})] \quad (3)$$

Where δ_i (i= 1,2,3,4) is empirical coefficient for each cell and C_{O2} is the dissolved oxygen concentration at the liquid/gas interface and is calculated by using the following expression

$$C_{O2} = \frac{P_{O2}}{\left(5.08\times10^{6}\right)\times exp(-498/T)} \quad (4)$$

Ohmic overvoltage V_{ohm} is expressed as

$$V_{ohm} = I_{FC}(R_C + R_M) \quad (5)$$

Where R_M is the electron flow equivalent resistance and R_C is the proton resistance. R_C is considered as constant.

$$R_M = \frac{\rho_m L}{A} \quad (6)$$

Where L is membrane thickness (cm), A denotes active area of membrane (cm^2) and ρ_m is the membrane specific resistivity (Ω-cm) and is given as

$$\rho_m = \frac{181.6\,[1 + 0.03J + 0.062(T/303)^2(J)2.5]}{[G - 0.634 - 3J]\ exp\,[4.18(1 - 303/T)]} \quad (7)$$

Where G is water content of the membrane and J is current density and is expressed as

$$J = \frac{I_{FC}}{A} \quad (8)$$

Finally, the concentration overvoltage V_{con} can be calculated from the following expression

$$V_{con} = -\frac{RT}{nF} ln\left(1 - \frac{J}{J_{max}}\right) \quad (9)$$

Where F is Faraday's constant, R is universal gas constant and J_{max} is maximum current density. A DC-DC converter is connected to the output of the fuel cell to maintain a constant voltage across the DC link. The design specifications of 1.26kW PEMFC are given in Table 1.

TABLE 1. 1.26kW PEMFC parameter specifications

Parameter Description	Rating
Maximum power (P_{max})	1.26 kW
Maximum current (I_{max})	52 A
Maximum voltage (V_{max})	24.23 V
Temperature (T)	55^0 C
Number of cells	42
Nominal air flow rate	2400 lpm

III. THREE-PHASE HIGH VOLTAGE GAIN IBC

The proposed converter consists of three switches (S_1, S_2 and S_3) and three diodes (D_1, D_2 and D_3). L_1, L_2 and L_3 are the filtering inductors of phase-1, phase-2 and phase-3 respectively. V_{FC} is the input voltage, V_O is output voltage and R is the load

This article has been accepted for publication in a future issue of this journal, but has not been fully edited. Content may change prior to final publication. Citation information: DOI 10.1109/ACCESS.2017.2785832, IEEE Access

resistor. The following assumptions are considered for the analysis of proposed high voltage gain IBC:

i. Inductors of all the three phases are assumed to be ideal (L_1= L_2 =L_3=L).

ii. Filtering capacitors C_1 and C_2 are considered as same (C_1 = C_2=C).

iii. The proposed converter always operates in Continuous Conduction Mode (CCM).

iv. The voltage and current ripples across the capacitor and inductor are assumed to be very small.

The switches S_1, S_2 and S_3 are switched ON by using two gate pulses which are 180˚ phase shifted. One gate pulse is given to the switch S_2 and another gate pulse with 180˚ phase shift is given to both the switches S_1 and S_3 [29]. Fig. 3 explains the operation of the proposed converter in different operating modes and the steady-state waveforms of this converter are shown in the Fig. 4.

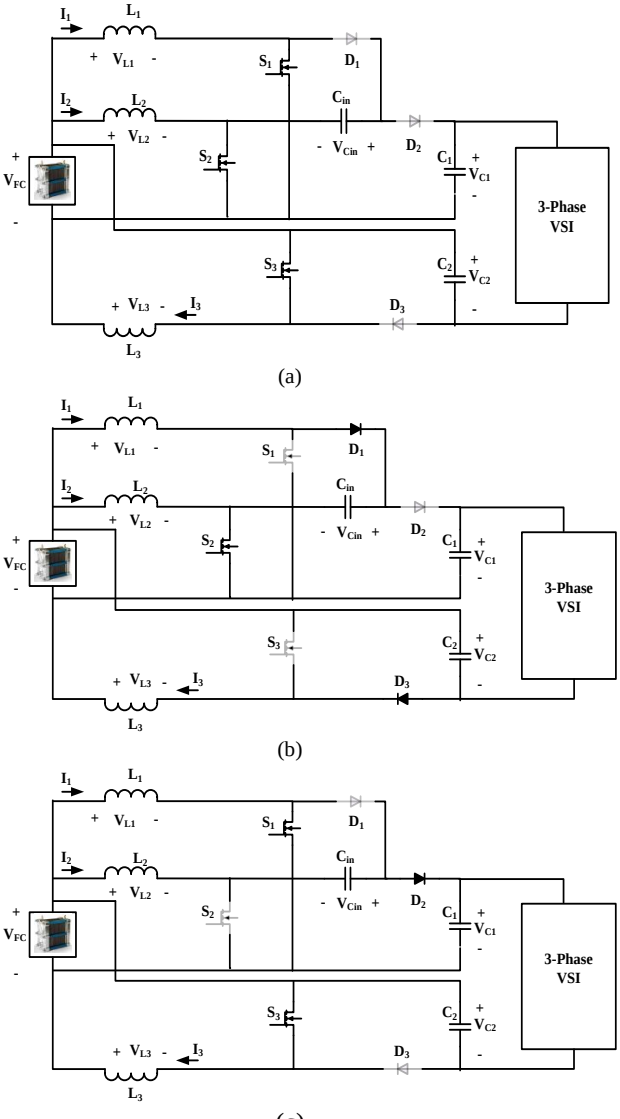

FIGURE 3. Modes of operation of 3-phase high voltage gain IBC.

Mode-1 ($t_o \le t \le t_1$): During this mode, all the three switches S_1, S_2 and S_3 are switched ON and all the three diodes D_1, D_2, and D_3 are reverse biased as shown in Fig. 3(a). The input voltage source V_{FC} charges the inductors L_1, L_2 and L_3. The current through these inductors I_1, I_2 and I_3 increased linearly with a slope of (V_{FC}/L). The input capacitor C_{in} is disconnected from the load as well as from the supply. The output capacitors C_1 and C_2 supplies energy to the load resistor and the voltage of output capacitors V_{C1} and V_{C2} decreases with a slope of (-V_O/RC).

Mode-2 ($t_1 \le t \le t_2$): In this mode, the switch S_2 is switched ON and the switches S_1 and S_3 are switched OFF. The diodes D_1 and D_3 are forward biased and the diode D_2 is reverse biased as shown in Fig. 3(b). The current through the inductors L_1 and L_3 decreased with a slope of (V_{FC} –V_{Cin})/L and (V_{FC} – V_{C2})/L respectively. The current through the inductor L_2 increases with a slope of (V_{FC}/L). The capacitor C_1 supplies the energy to the load and the capacitors C_2 and C_{in} are charged by the input voltage V_{FC}.

Mode-3 ($t_3 \le t \le t_4$): This mode is similar to mode-1. All the three switches S_1, S_2 and S_3 are switched ON and all the three diodes D_1, D_2 and D_3 are switched OFF.

Mode-4 ($t_4 \le t \le t_5$): In this mode, the switch S_2 is switched OFF and the switches S_1 and S_3 are switched ON. The diodes D_1 and D_3 are reverse biased and the diode D_2 is conducting as shown in Fig. 3(c). The input voltage source V_{FC} charges the inductors L_1 and L_3 and the current through these inductors increases with a slope of (V_{FC}/L). The current through the inductor L_2 decreases with a slope of (V_{FC}+V_{Cin}-V_{C1})/L. The capacitors C_2 and C_{in} supplies energy to the load. Capacitor C_1 gets charged by the input voltage V_{FC}.

A. ANALYSIS OF THE CONVERTER

To simplify the analysis of the converter, inductors, capacitors and power semiconductor devices are assumed to be ideal and the converter operating in CCM.

The static voltage gain (M) of the DC-DC converter is obtained by applying volt-second balance on inductors L_1, L_2 and L_3. By applying volt-second balance to the inductor L_1, we get

$$V_{L1} = V_{FC}(t_1 - t_O) + (V_{FC} - V_{Cin})(t_2 - t_1) + V_{FC}(t_3 - t_2) + V_{FC}(t_4 - t_3) = 0 \quad (10)$$

From Eq. (10), input capacitor voltage V_{Cin} is obtained as

$$V_{Cin} = \frac{V_{FC}}{(1-D)} \quad (11)$$

By applying volt-second balance to the inductor L_2, we get

This article has been accepted for publication in a future issue of this journal, but has not been fully edited. Content may change prior to final publication. Citation information: DOI 10.1109/ACCESS.2017.2785832, IEEE Access

$$V_{L2} = V_{FC}(t_1 - t_O) + V_{FC}(t_2 - t_1) + V_{FC}(t_3 - t_2) + (V_{FC} + V_{Cin} - V_{C1})(t_4 - t_3) = 0 \quad (12)$$

Solving Eq. (12) yields

$$V_{C1} = \frac{V_{FC}}{(1-D)} + V_{Cin} \quad (13)$$

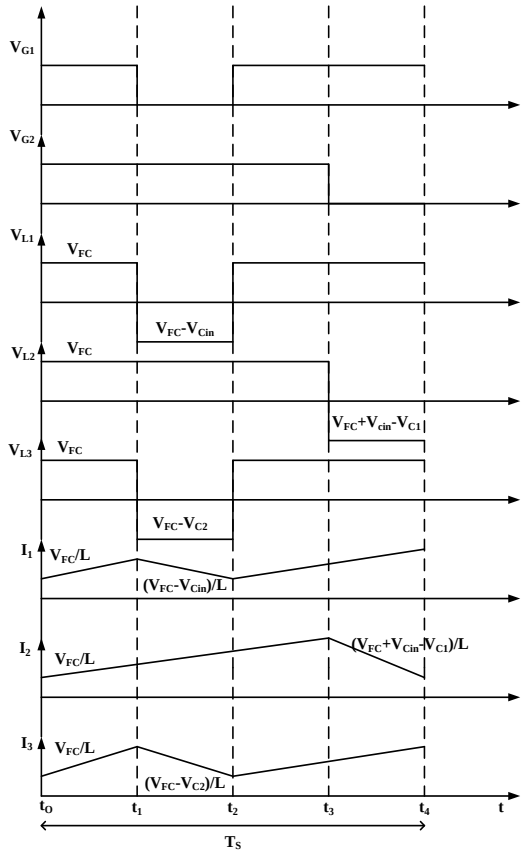

FIGURE 4. Steady-state waveforms of 3-Phase high voltage gain IBC.

From Eq. (11) and Eq. (13) we get

$$V_{C1} = \frac{2V_{FC}}{(1-D)} \quad (14)$$

By applying volt-second balance to the inductor L_3, we get

$$V_{L3} = V_{FC}(t_1 - t_O) + (V_{FC} - V_{C2})(t_2 - t_1) + V_{FC}(t_3 - t_2) + V_{FC}(t_4 - t_3) = 0 \quad (15)$$

From Eq. (15), capacitor C_2 voltage is obtained as

$$V_{C2} = \frac{V_{FC}}{(1-D)} \quad (16)$$

The output voltage of the converter is obtained by using the Eq. (17)

$$V_O = V_{C1} + V_{C2} - V_{FC} \quad (17)$$

From Eqs. (14) (16) and (17), the converter static voltage gain M is obtained as

$$M = \frac{V_O}{V_{FC}} = \frac{(2+D)}{(1-D)} \quad (18)$$

Fig.5 shows the voltage gain comparison of the proposed converter with conventional two-phase IBC.

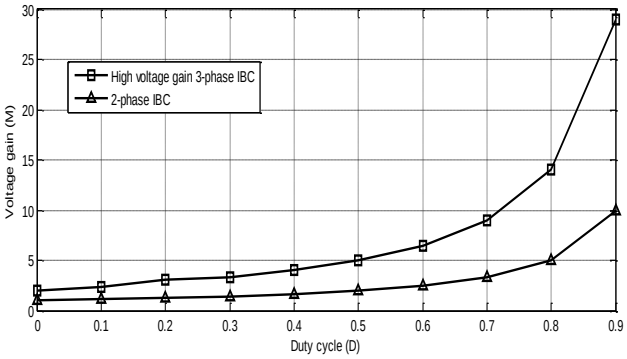

FIGURE 5. Voltage gain comparison of 3-phase high voltage gain IBC with 2-phase IBC.

The switches S_1 and S_3 are switched OFF in mode-2 and remains switched ON in all the other modes. From Fig. 3(b), the voltage stress of switches S_1 and S_2 can be expressed as

$$V_{S1} = V_{Cin} = \frac{V_{FC}}{(1-D)} \quad (19)$$

$$V_{S2} = V_{C1} - V_{Cin} = \frac{V_{FC}}{(1-D)} \quad (20)$$

The switch S_2 is switched OFF in only mode-4. From Fig. 3(c), the voltage stress of switch S_3 is expressed as

$$V_{S3} = V_{C2} = \frac{V_{FC}}{(1-D)} \quad (21)$$

In the same way the voltage stress of the diodes D_1, D_2 and D_3 can be derived and they expressed as

$$V_{D1} = -V_{C1} = -\frac{2V_{FC}}{(1-D)} \quad (22)$$

$$V_{D2} = V_{Cin} - V_{C2} = -\frac{V_{FC}}{(1-D)} \quad (23)$$

$$V_{D3} = V_{C2} = \frac{V_{FC}}{(1-D)} \quad (24)$$

Inductance L is designed by using the input current ripple (ΔI). The maximum input current ripple is assumed as 20% of the input current. The value of the input inductor is calculated by using the Eq. (25).

$$L = L_1 = L_2 = L_3 = \frac{DV_{FC}}{\Delta I f_S} \quad (25)$$

Similarly, the input and output capacitors are designed by using the voltage ripples across the input and output capacitors. The voltage ripple (ΔV) is considered as 10% of the input voltage.

$$C_{in} = \frac{V_O}{R\Delta C_{in} f_S} \quad (26)$$

$$C = C_1 = C_2 = \frac{DV_O}{R\Delta V f_S} \quad (27)$$

This article has been accepted for publication in a future issue of this journal, but has not been fully edited. Content may change prior to final publication. Citation information: DOI 10.1109/ACCESS.2017.2785832, IEEE Access

IV. CONTROLLER DESIGN

Two control strategies are used for the proposed configuration. One is for to track the maximum power of the fuel cell and another one is for BLDC motor operation.

A. RBFN BASED MPPT CONTROLLER

MPPT is needful for fuel cell system to extract the maximum power from it at different temperature conditions. For the proposed configuration RBFN based MPPT controller is developed and the results are compared with FLC.

RBFN is a type of feedforward neural network model and has both supervised and unsupervised learning phases. RBFN typically consists of three layers: an input layer, a hidden layer and an output layer as shown in Fig.6. The hidden layer consists of non-linear radial basis activation function whereas the output layer is linear one [30].

The nodes in the input layer are used to transmit the inputs to the hidden layer [31-32]. The net input and output of the input neuron are represented as

$$x_i^{(1)}(n) = net_i^{(1)} \tag{28}$$

$$y_i^{(1)}(n) = f_i^{(1)}[net_i^{(1)}(n)] = net_i^{(1)}(n),\ i = 1,2 \tag{29}$$

Where $x_i^{(1)}$ is input layer, $y_i^{(1)}$ is hidden layer and $net_i^{(1)}$ is sum of the input layer. Every node in the hidden layer performs as Gaussian function. The Gaussian function is used as a membership function in the RBFN.

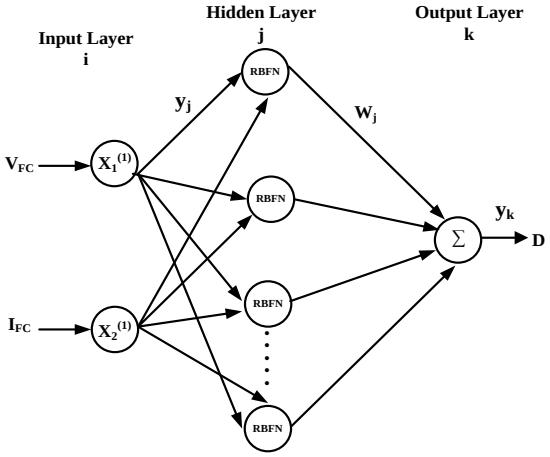

FIGURE 6. RBFN structure.

$$net_j^{(2)}(n) = -\left(X - M_j\right)^T \sum_j (X - M_j) \tag{30}$$

$$y_j^{(2)}(n) = f_j^{(2)}[net_j^{(2)}(n)]\ exp[net_j^{(2)}(n)],\ j = 1,2,..... \tag{31}$$

Where M_j and $\sum_j$ are mean and standard deviation of the Gaussian function respectively. The output layer has single node k, generates the linear control signal (D).

$$net_k^{(3)} = \sum_j w_j y_j^{(2)} \tag{32}$$

$$y_k^{(3)} = f_k^{(3)}[net_k^{(3)}(n)] = net_k^{(3)}(n) \tag{33}$$

Where w_j is the connective weight matrix between output and hidden layer. In this paper current and voltage of fuel cell are taken as inputs to the RBFN controller and it produces duty cycle (D) as the output as shown in Fig. 7.

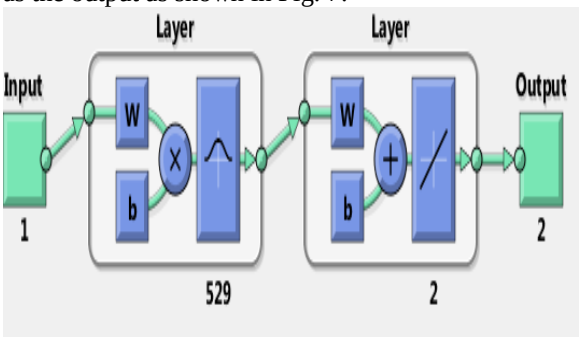

FIGURE 7. RBFN based MPPT architecture for the fuel cell.

B. ELECTRONIC COMMUTATION

The control signals to the switches of the VSI are obtained from the BLDC motor electronic commutation [33-34]. Three hall sensors are used to generate three hall signals depending on the motor rotor position for each interval of 60˚. These generated hall signals are converted into switching pulses to the VSI by using a decoder circuit. The switching states of VSI are listed in Table 2.

TABLE 2. Switching states for electronic commutation of BLDC motor

Θ (deg)	Hall Signals			Switching States					
	H_1	H_2	H_3	S_4	S_5	S_6	S_7	S_8	S_9
NA	0	0	0	0	0	0	0	0	0
0-60	1	0	1	1	0	0	1	0	0
60-120	1	0	0	1	0	0	0	0	1
120-180	1	1	0	0	0	1	0	0	1
180-240	0	1	0	0	1	1	0	0	0
240-300	0	1	1	0	1	0	0	1	0
300-360	0	0	1	0	0	0	1	1	0
NA	1	1	1	0	0	0	0	0	0

V. SIMULATION AND RESULT ANALYSIS

The performance of the proposed BLDC motor driven FCEV system is analyzed by using the MATLAB/Simulink platform. To analyze the dynamic response of the FCEV system, sudden changes in the temperature of the fuel cell is considered as follows: T= 320˚K for a period of 0 to 0.3sec, T= 310˚K for a period of 0.3 sec to 0.6 sec and T= 330˚K for a period of 0.6sec to 0.9 sec as shown in Fig. 8.

For the different temperatures the output current, voltage and power waveforms of the fuel cell are as shown in Fig. 9. Fuel cell generates a power of 1080W for 0 to 0.3 sec, 970W for 0.3sec to 0.6 sec and 1220W for 0.6sec to 0.9sec.

Fig. 10 shows The DC link current, voltage and power by using the FLC base MPPT technique. It generates a power of 1000W, 830W and 1150W for the temperatures of 320˚K, 310˚K and 330˚K respectively. The DC link output current, voltage and power using proposed RBFN based MPPT controller are shown in the Fig. 11. The proposed controller gives 1050W for the temperature of 320˚K, 900W for 310˚K and 1200W for the temperature of 330˚K. In Fig. 12, the performance of the RBFN based MPPT controller for fuel cell is compared with fuzzy logic based MPPT controller. From Fig. 12, it is observed that proposed controller generates the high DC link power than the FLC. The comparative analysis of FLC and RBFN controllers are listed in Table 3.

The starting and steady-state characteristics of the BLDC motor at different temperatures of the fuel cell are as shown in the Fig. 13. The motor parameters such as stator current (Isa), back EMF (E), electromagnetic torque (Te) and load torque (T_L) are presented at dynamic temperature conditions of the fuel cell. The BLDC motor has a speed of 3300 rpm for 0 to 0.3sec, 2400 rpm for 0.3sec to 0.6sec and 3700 rpm for 0.6sec to o.9sec. The torque of the BLDC motor remains constant for varying speed conditions.

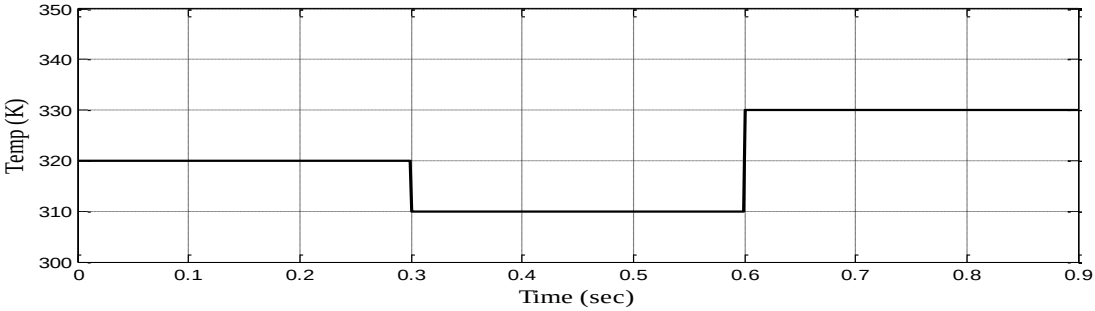

FIGURE 8. Temperature changes in PEMFC system.

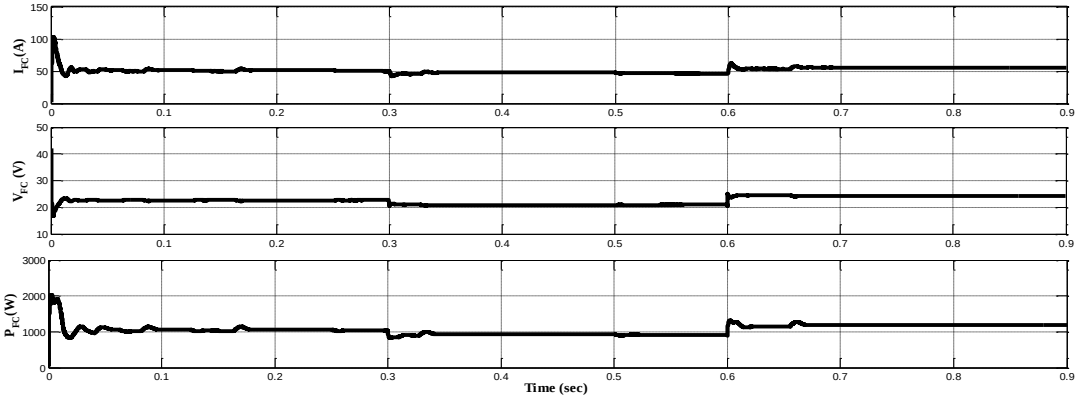

FIGURE 9. Fuel cell output current, voltage and power at different temperatures.

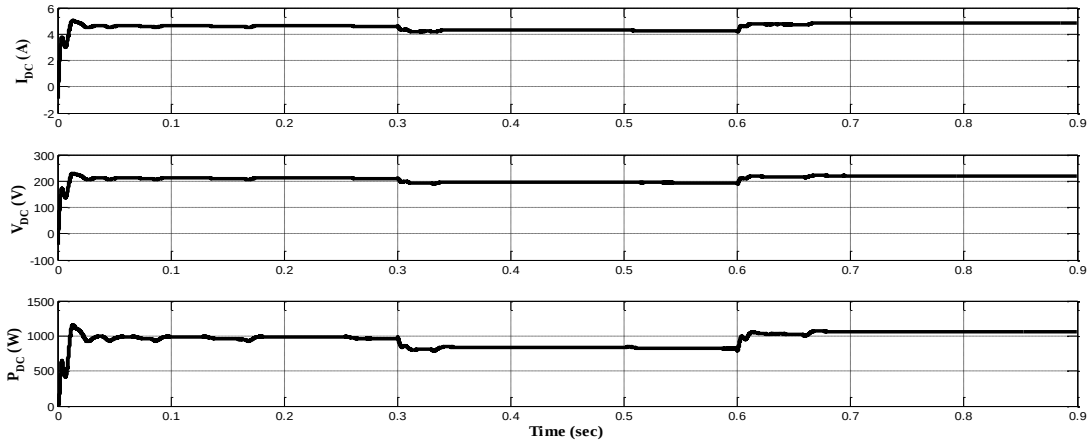

FIGURE 10. DC link output current, voltage and power at different temperatures using FLC.

This article has been accepted for publication in a future issue of this journal, but has not been fully edited. Content may change prior to final publication. Citation information: DOI 10.1109/ACCESS.2017.2785832, IEEE Access

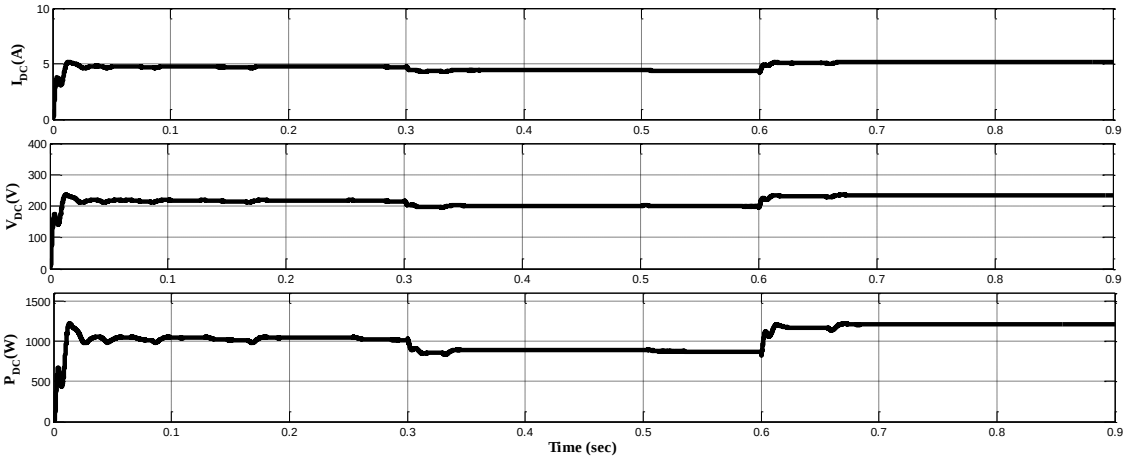

FIGURE 11. DC link output current, voltage and power at different temperatures using RBFN.

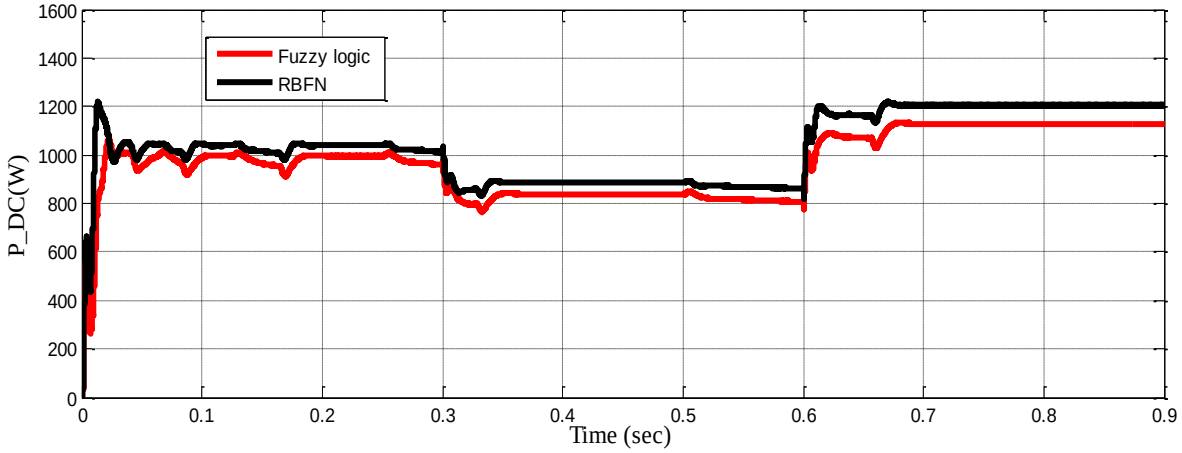

FIGURE 12. Comparison of DC link power with both RBFN and Fuzzy based MPPT controllers.

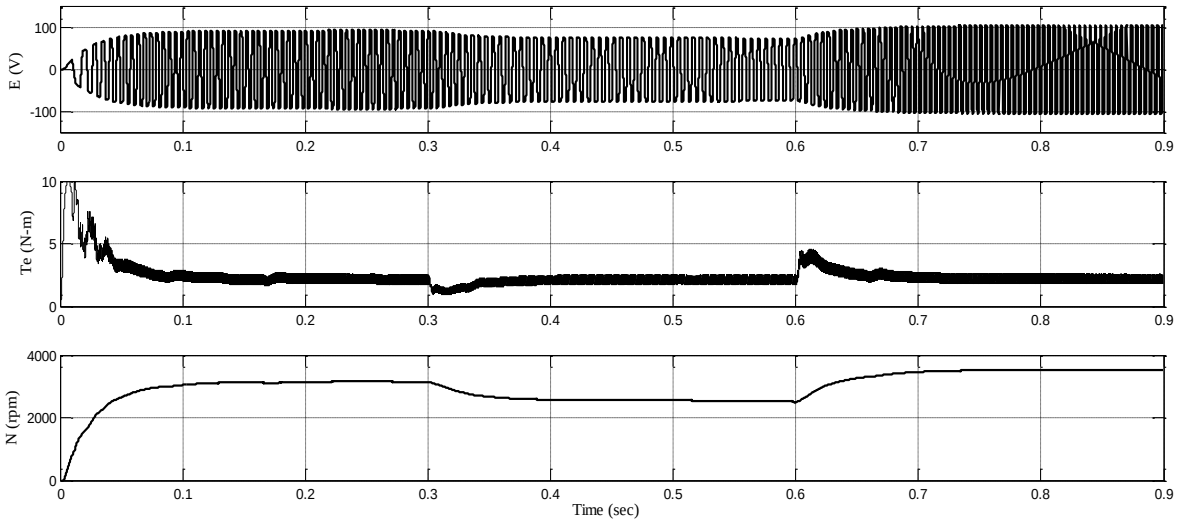

FIGURE 13. BLDC motor parameters.

TABLE 3. Comparison of DC link power with both RBFN and Fuzzy based MPPT controllers

Parameter	1.26 kW PEMFC with fuzzy based MPPT			1.26 kW PEMFC with RBFN based MPPT		
Period (sec)	0 to 0.3	0.3 to 0.6	0.6 to 0.9	0 to 0.3	0.3 to 0.6	0.6 to 0.9
Fuel cell temperature (˚K)	320	310	330	320	310	330
DC link current (A)	4.71	4.3	5.1	4.8	4.4	5.21
DC link voltage (V)	212	193	225	220	205	230
DC link power (W)	1000	830	1150	1050	900	1200

VI. CONCLUSION

In this paper, a three-phase high voltage gain DC-DC converter is proposed for FCEV applications. The proposed converter has reduced the fuel cell input current ripples and the voltage stress on the power semiconductor switches. The RBFN based MPPT technique is designed for 1.26 kW PEMFC for extracting the maximum power from the fuel cell at different temperatures. The proposed MPPT technique is compared with the FLC MPPT controller. The simulation results reveal that the RBFN based MPPT controller has tracked the maximum power point faster when compared to the fuzzy logic controller. Also, different performance characteristics of the BLDC motor such as electromagnetic torque, speed and back EMF are analyzed at different temperatures of the fuel cell system.

REFERENCES

[1] Chiu, H.J. and Lin, L.W. "A bidirectional DC–DC converter for fuel cell electric vehicle driving system." *IEEE Trans Power Electron.*, vol.21(4), pp.950-958, 2006.

[2] Geng, B., Mills, J.K. and Sun, D. "Combined power management/design optimization for a fuel cell/battery plug-in hybrid electric vehicle using multi-objective particle swarm optimization." *Inter J Automot Techn.*, vol.15(4), pp.645-654, 2014.

[3] Hemi H, Ghouili J, Cheriti A. "A real time fuzzy logic power management strategy for a fuel cell vehicle". *Energy Convers. Manag.*, vol. 80, pp. 63-70,2014.

[4] Mebarki, N., Rekioua, T., Mokrani, Z., Rekioua, D. and Bacha, S. "PEM fuel cell/battery storage system supplying electric vehicle." *Int J of Hydrogen Enery*., vol41(45), pp.20993-21005, 2016.

[5] Abdi, Sh, K. Afshar, N. Bigdeli, and S. Ahmadi. "A novel approach for robust maximum power point tracking of PEM fuel cell generator using sliding mode control approach." *Int. Jou. Elec. Sci*., pp. 4192-4209, 2012

[6] Esram T, Chapman PL. "Comparison of photovoltaic array maximum power point tracking techniques." *IEEE Trans Energy Conver*., vol.22(2), pp.439-49, 2007

[7] Saravanan S, Babu NR. "Maximum power point tracking algorithms for photovoltaic system–A review", *Renew Sustain Energy Rev.*, vol. 57, pp. 192-204, 2016.

[8] Ram JP, Rajasekar N, Miyatake M. "Design and overview of maximum power point tracking techniques in wind and solar photovoltaic systems: *Renew Sustain Energy Rev.*, vol. 73, pp. 1138-1159, 2017.

[9] Khanh LN, Seo JJ, Kim YS, Won DJ. "Power-management strategies for a grid-connected PV-FC hybrid system." *IEEE Trans Power Deliver*., vol.25(3), pp. 1874-1882, 2010.

[10] Giustiniani A, Petrone G, Spagnuolo G, Vitelli M. "Low-frequency current oscillations and maximum power point tracking in grid-connected fuel-cell-based systems." *IEEE Trans Indus Electron*., vol. 57(6), pp. 2042-2053, 2010.

[11] Kumar, K., N. Ramesh Babu, and K. R. Prabhu. "Design and Analysis of an Integrated Cuk-SEPIC Converter with MPPT for Standalone Wind/PV Hybrid System." *Int. J Renewable Energy Research*, vol. 7, pp. 96-106, 2017.

[12] Kumar K, Babu NR, Prabhu KR. "Design and Analysis of RBFN-Based Single MPPT Controller for Hybrid Solar and Wind Energy System". *IEEE Access*., vol. 5, pp.15308-15317, 2017

[13] Sobrino-Manzanares F, Garrigós A. "An interleaved, FPGA-controlled, multi-phase and multi-switch synchronous boost converter for fuel cell applications." *Int J of Hydrogen Enery*., vol.40 (36), pp. 12447-56, 2015.

[14] Haroun, R., El Aroudi, A., Cid-Pastor, A. and Martinez-Salamero, L. "Sliding Mode Control of output-parallel-connected two-stage boost converters for PV systems." In Systems, Signals & Devices (SSD), 2014 11th International Multi-Conference on (pp. 1-6), 2014.

[15] Ye, Y.M. and Cheng, K.W.E." Quadratic boost converter with low buffer capacitor stress." *IET Power Electron.*, vol.7(5), pp.1162-1170, 2013.

[16] Shahin, A., Huang, B., Martin, J.P., Pierfederici, S. and Davat, B. "New non-linear control strategy for non-isolated DC/DC converter with high voltage ratio." *Energy Convers. Manag.*, vol.51(1), pp.56-63, 2010.

[17] Shahin, A., Hinaje, M., Martin, J.P., Pierfederici, S., Rael, S. and Davat, B. "High voltage ratio DC–DC converter for fuel-cell applications." *IEEE Trans Indus Electron*., vol. 57(12), pp.3944-3955, 2010.

[18] Alcazar, Y.J.A., Bascopé, R.T., de Oliveira, D.S., Andrade, E.H. and Cárdenas, W.G. "High voltage gain boost converter based on three-state switching cell and voltage multipliers." In Industrial Electronics, 34th Annual Conference of IEEE, *IECON* ,pp. 2346-2352 , 2008.

[19] Tofoli, F.L., de Souza Oliveira, D., Torrico-Bascope, R.P. and Alcazar, Y.J.A. "Novel nonisolated high-voltage gain dc–dc converters based on 3SSC and VMC." *IEEE Trans Power Electron*., vol.27(9), pp.3897-3907, 2012.

[20] Li, W., Zhao, Y., Wu, J. and He, X. "Interleaved high step-up converter with winding-cross-coupled inductors and voltage multiplier cells." *IEEE Trans Power Electron.*, vol 27(1), pp.133-143, 2012.

[21] Hsieh, Y.P., Chen, J.F., Liang, T.J. and Yang, L.S. "A novel high step-up DC–DC converter for a microgrid system." *IEEE Trans Power Electron.*, vol.26(4), pp.1127-1136, 2011.

[22] Li, W., Li, W., He, X., Xu, D. and Wu, B. "General derivation law of non-isolated high-step-up interleaved converters with built-in transformer." *IEEE Trans Indus Electron.*, vol.59(3), pp.1650-1661, 2012.

[23] Singh B, Kumar R. "Solar photovoltaic array fed water pump driven by brushless DC motor using Landsman converter." *IET Renew Power Gen*., vol. 10(4), pp. 474-84, 2016.

[24] Singh B, Bist V. "A BL-CSC converter-fed BLDC motor drive with power factor correction". *IEEE Trans Indus Electron*., vol. 62(1) pp. 172-83, 2015.

[25] Benyahia N, Denoun H, Zaouia M, Rekioua T, Benamrouche N. "Power system simulation of fuel cell and supercapacitor

based electric vehicle using an interleaving technique." *Int J of Hydrogen Enery*., vol. 40(45), pp. 15806-15814. 2015.

[26] Mebarki N, Rekioua T, Mokrani Z, Rekioua D, Bacha S. "PEM fuel cell/battery storage system supplying electric vehicle." *Int J of Hydrogen Enery*., vol. 41(45), pp. 20993-21005. 2016.

[27] Priya K, Babu TS, Balasubramanian K, Kumar KS, Rajasekar N. " A novel approach for fuel cell parameter estimation using simple Genetic Algorithm." Sustain Energy Techno Assessment, vol.31(12), pp.46-52, 2015.

[28] Rajasekar N, Jacob B, Balasubramanian K, Priya K, Sangeetha K, Babu TS. "Comparative study of PEM fuel cell parameter extraction using Genetic Algorithm." Ain Shams Engineering Journal, vol.6(4), pp.1187-1194. 2015.

[29] Farooq A, Malik Z, Qu D, Sun Z, Chen G. "A three-phase interleaved floating output boost converter." *Adv Mater Eng*., 2015.

[30] Saravanan, S., and N. Ramesh Babu. "RBFN based MPPT algorithm for PV system with high step up converter." *Energy Convers. Manag.*, vol. 122, pp. 239-251, 2016.

[31] Rai AK, Kaushika ND, Singh B, Agarwal N. "Simulation model of ANN based maximum power point tracking controller for solar PV system." *Sol Energ Mat a Sol C*., vol. 95(2), pp. 773-778, 2011.

[32] Seshagiri S, Khalil HK. "Output feedback control of nonlinear systems using RBF neural networks." *IEEE Trans Neural Networ*., vol. 11(1), pp. 69-79, 2000.

[33] Bist V, Singh B. "Reduced sensor configuration of brushless DC motor drive using a power factor correction-based modified-zeta converter." *IET Power Electron*., vol.7(9), pp. 2322-2335, 2014.

[34] Singh B, Kumar R. "Simple brushless DC motor drive for solar photovoltaic array fed water pumping system." *IET Power Electron*., vol. 9(7), pp. 1487-1495, 2016.